IOP Publishing Journal of Physics B: Atomic, Molecular and Optical Physics
J. Phys. B: At. Mol. Opt. Phys. **53** (2020) 085603 (11pp) https://doi.org/10.1088/1361-6455/ab7523

Laser intensity effect on the dissociation of vibrationally excited D_2^+ in intense fields at 792 and 198 nm

Z M Jia[1,3], Q Y Yue[2] and Y D Peng[1,3]

[1] College of Electronic and Information Engineering, Shandong University of Science and Technology, Qingdao, 266590, People's Republic of China
[2] Shandong Provincial Engineering and Technical Center of Light Manipulations & Shandong Provincial Key Laboratory of Optics and Photonic Device, School of Physics and Electronics, Shandong Normal University, Jinan, 250358, People's Republic of China

E-mail: jiazhengmao@siom.ac.cn and pengyd@sdust.edu.cn

Received 10 September 2019, revised 11 January 2020
Accepted for publication 11 February 2020
Published 24 March 2020

Abstract

We investigate the field intensity effect on the dissociation of vibrating D_2^+ in intense laser pulses at two central wavelengths (792 and 198 nm) by numerically solving the non-Born–Oppenheimer time-dependent Schrödinger equation and the coupled equations among electronic states. The dissociation degree oscillates with increasing intensity of the interaction field, which can be explained with the Floquet representation. Besides, the Rabi oscillations can also be used to reveal the underlying mechanism of the population oscillations: the Rabi frequency will be increased with the increase of the external pulse, which leads to the oscillations of the dissociation populations. When a single cycle terahertz pulse with a central wavelength of 36 μm is used to steer the electron motion after the excitation of the 792 and 198 nm pulses, about 97.6%, respectively, 92.1% electron populations of all the dissociation events can be localized at one potential well.

Keywords: laser induced molecular dissociation, vibrationally excited D_2^+, non-Born–Oppenheimer time-dependent Schrödinger equation, Floquet representation, Rabi oscillation

(Some figures may appear in colour only in the online journal)

1. Introduction

The interactions of diatomic molecules with ultrashort intense laser pulses can yield very complex dynamics, one of which is molecular dissociation. With H_2^+ and its isotopes, people have unveiled a series of interesting scenarios about laser induced molecular dissociation, such as bond softening (BS) [1–3], bond hardening (BH) [4–6], above threshold dissociation [7, 8], multiphoton dissociation [8, 9], zero-photon dissociation [10, 11], and so on [6, 8, 12].

With the time-dependent Schrödinger equation (TDSE) of a two-state model, one can find that the dissociation probability of the field-aligned H_2^+, whose initial state of the vibrational level is $\nu = 5$, shows an increasing trend with increasing intensity of the external field with a central wavelength in the proximity of 780 nm. While the populations of the dissociation state drop off obviously at some intensities, due to trapping in one- and three-photon field induced adiabatic potential wells [13, 14]. With the non-Born–Oppenheimer (non-BO) TDSE, the dissociation probability of H_2^+ shows only one peak value with increasing intensity of the 800 nm pulse (there is only one maximum dissociation probability and then monotonic decrease due to ionization), when the ground state (electronic $1s\sigma_g$ state and vibrational $\nu = 0$ state) is chosen to be the initial state [15]. The simulation results show that, at low field intensities, the dissociation ratio increases monotonously with increasing intensity of the external pulse. However, at high intensities, the dissociation probability shows a monotonous decrease with a continuous increase of the pulse intensity, because more and more electron populations are ionized away.

[3] Authors to whom any correspondence should be addressed.

There are two experimental methods for preparing H_2^+ and its isotopes: the ionization of the corresponding neutral molecule with a pump pulse [16–18] or by high energy electron impact [19–21]. When H_2^+ is produced by the ionization of H_2 on the leading edge of a laser pulse, the relative populations of the vibrational levels of the molecular ion are found to be concentrated in the lowest vibrational levels [16]. Whereas, the single ionization of H_2 by an extreme ultraviolet (UV) attosecond pulse train [17], a strong infrared (IR) pulse [18] or an electron impact [19–21] will lead to a Franck–Condon (FC) distribution of the H_2^+ vibrational manifold. In the present work, we consider the case of incoherent FC distribution [22–26]. Results obtained with this case agree well with the experimental results [27], though the time-evolving phase factor of each vibrational state is ignored [17]. In the paper, a systematic investigation of the pulse intensity dependence in the laser induced dissociation of a vibrating D_2^+ is reported. The central wavelengths of the few-cycle exciting pulses are 792 nm and 198 nm, respectively. The dissociation degree oscillates with increasing intensity of the external field. The population oscillating can be explained with BS [1–3] and BH [4–6]. Besides, this oscillating phenomenon can also be explained with the Rabi oscillations, which can take place both in atoms and molecules [26–33].

The electron populations can be driven back and forth between the two nuclei in the laser induced dissociating D_2^+. When the inter-nuclear potential barrier becomes too large for the electron to tunnel, it is stabilized at one of the two potential wells. This is the so-called laser induced dissociation control, and attracts much attention since the landmark experiment of Kling *et al* who observed the asymmetric electron distribution in the dissociating D_2^+ by utilizing a few-cycle phase-stabilized pulse [22, 34–39]. For a single 800 nm multicycle pulse, about 70.0% populations of all t he dissociation events can be steered onto one potential well in the laser-induced dissociation control of the vibrating molecular ion D_2^+. Whereas, the asymmetry distribution can be significantly smeared out in the few-cycle regime, because different vibrational states exhibit different carrier-envelope phase (CEP) dependences [24, 39]. In the present work, we utilize a single cycle 36 μm terahertz (THz) pulse to steer the electron motion after the one-photon resonant excitation of a short few-cycle 792 nm IR pulse or after the two-photon resonant excitation of a short few-cycle 198 nm UV pulse, about 97.6%, respectively, 92.1% populations of all the dissociation states can be stabilized at one potential well at the end of the simulation, even though more than half the populations of all the dissociation events are localized at the $2s\sigma_g$ state after the exciting of the UV field.

This paper is organized as follow: section 2 describes briefly the model system of the vibrating D_2^+. In section 3, the numerical results for the exploration of the 792 nm pulse strength dependence landscape of electron dynamics are studied. And the physical mechanism underlying is demonstrated with the Floquet representation [40, 41] and the coupled equations (CEs) of the four lowest electronic states [42]. The involvement of higher excited states with the dependence of the dissociation degree on the 198 nm UV pulse strength is studied in section 4. Section 5 describes the advantages of a single optical cycle 36 μm THz laser pulse as a steering field in the dissociation control of the vibrating D_2^+. Finally, a brief summary and conclusions are contained in section 6.

2. Simulation model

In order to obtain the dynamics of the molecular ion D_2^+, the three-body non-BO TDSE with both electronic and nuclear degrees of freedom should be numerically solved. A real nine-dimensional TDSE is beyond the current capability, therefore, a reduced model is usually used [43–45]. The molecular rotation of D_2^+, whose time scale is several hundreds of femtoseconds, can be neglected in the ultrashort laser fields. When the molecular axis and the electron movement direction are restricted to the polarization direction of the external fields, we can use a two-dimensional (one molecular plus one electronic degree of freedom) model to conduct the simulation. This model agrees well with the three-dimensional model, even though some quantitative deviations exist [46]. The corresponding non-BO TDSE can be written as ($e = \hbar = 1$ in atomic unit (a.u.), which are used throughout the paper unless otherwise stated) [43–45]

$$i\frac{\partial}{\partial t}\Psi_\nu(R, z; t) = [H_0(R, z; t) + W(z, t)]\Psi_\nu(R, z; t), \quad (1)$$

with

$$H_0(R, z; t) = -\frac{1}{m_d}\frac{\partial^2}{\partial R^2} + \frac{1}{R} - \left(\frac{2m_d + m_e}{4m_d m_e}\right)\frac{\partial^2}{\partial z^2} - \frac{1}{\sqrt{(z + R/2)^2 + 1}} - \frac{1}{\sqrt{(z - R/2)^2 + 1}}. \quad (2)$$

Here $\Psi_\nu(R, z; t)$ is the temporal wave function corresponding to the νth vibrational level. m_e, respectively, m_d are the electron mass and nucleus mass ($m_e = 1$, $m_d = 3674$). Throughout the paper, R and z collectively represent the relative inter-nuclear distance and the electronic coordinate with respect to the center of mass of the two nuclei, respectively. $W(z, t)$ indicates the interaction of the particle with the external laser field, which can be described as

$$W(z, t) = \left(1 + \frac{m_e}{2m_d + m_e}\right)zE(t), \quad (3)$$

where $E(t)$ is the time dependent electric component of the external exciting field, which is defined by the vector potential $A(t) = -E_0/\omega \sin(\pi t/T)^2 \cos(\omega t + \phi_{\rm CEP})$. Then $E(t)$ can be expressed as $E(t) = -\partial A(t)/\partial t$, here E_0 is the peak electric field amplitude in atomic units, T is the pulse duration, ω is the central frequency and $\phi_{\rm CEP}$ is the CEP of the external pulse, respectively. In this work, $\phi_{\rm CEP}$ is chosen as zero.

In our simulation, each vibrational state of the molecular ion D_2^+ is weighted by a constant coefficient C_ν, whose square is known as FC factors [24, 25]. Then the initial wave function corresponding to the νth vibrational level can be

expressed as

$$\Psi_\nu(R, z; 0) = C_\nu \chi_\nu(R)\phi(R, z), \tag{4}$$

with $\chi_\nu(R)$ being the νth eigenstate of the nuclear bound on the lowest potential curve in the BO approximation. The electronic wave function $\phi(R, z)$ is found by solving the Schrödinger equation at each fixed inter-nuclear distance R by using the imaginary time propagation method [47]. The contribution coefficient C_ν refers to [48]. With the second-order split-operator technique [49], the temporal wave function $\Psi_\nu(R, z; t)$ can be obtained by solving equation (1) numerically on a two-dimensional grid which contains 4096 points on the z axis with a step of 0.3 a.u. and 4096 points on the R axis with a step of 0.05 a.u. The time step is set to 0.05 a.u. A masking function $\cos^{1/8}$ is employed in the simulation, which can avoid spurious reflections of the wave packets from the three boundaries (one boundary of the R axis plus two boundaries of the z axis). The time-dependent total wave function satisfies $|\Psi(R, z; t)|^2 = \sum_\nu |\Psi_\nu(R, z; t)|^2$ [24–26, 39].

The dissociation probability of D_2^+ is defined as [39]

$$P_p = \int_{10.0}^{R_{\max}} dR \int_{-R/2.0-5.0}^{R/2.0+5.0} dz |\Psi(R, z; t_{end})|^2, \tag{5}$$

where $R_{\max}$ is the boundary of the R axis and $\Psi(R, z; t_{end})$ corresponds to the final wave function. In our simulation, t_{end} is taken at 120 fs after the on-set of the external pulse, the electron-nuclear stabilization is stable then. The total ionization probability can be set as $P_i = 1.0 - E_{sr}$, with $E_{sr} = \int_{0.0}^{R_{\max}} dR \int_{-z_{\max}}^{z_{\max}} dz\, |\Psi(R, z; t_{end})|^2$ being the final electron survival probability, and $\pm z_{\max}$ are the two boundaries of the z axis.

The temporal populations of the ith electronic state of the dissociating D_2^+ can be expressed as [50]

$$D_i(t) = \sum_\nu \int_0^{R_{\max}} dR \int_{-z_{\max}/2}^{z_{\max}/2} dz\, |\psi_{\nu,i}(z, R; t)|^2, \tag{6}$$

here $\psi_{\nu,i}(z, R; t)$ is the electron wave function of the ith electronic state, which is obtained by projecting the temporal electron-nuclear wave function $\Psi_\nu(R, z; t)$ of the νth vibrational level onto the ith electronic bound state $\phi_i(R, z)$

$$\psi_{\nu,i}(R, z; t) = \phi_i(R, z) \int_0^{R_{\max}} dR \int_{-z_{\max}}^{z_{\max}} \Psi_\nu^*(R, z; t)\phi_i \times (R, z)dz. \tag{7}$$

Here, i equals to 0, 1, 2 and 3, corresponds to the $1s\sigma_g$, $2p\sigma_u$, $2s\sigma_g$ and $3p\sigma_u$ states of D_2^+, respectively.

Under the BO approximation, the molecular wave function of D_2^+ corresponding to the νth vibrational level is written as [33]

$$\Psi_\nu(R, z; t) = \sum_m \chi_m^\nu(R, t)\phi_m(R, z), \tag{8}$$

here $\chi_m^\nu(R, t)$ represents the nuclear wave packet, and $\phi_m(R, z)$ is the corresponding electronic state. Inserting equation (8) into the TDSE yields the governing equation of the CEs among the electronic states of D_2^+

$$i\frac{\partial}{\partial t}\begin{pmatrix} \chi_1^\nu \\ \chi_2^\nu \\ \cdot \\ \chi_m^\nu \\ \cdot \end{pmatrix} = \begin{pmatrix} T+V_1 & D_{1,2} & \cdot\ \cdot & D_{1,m} & \cdot\ \cdot \\ D_{2,1} & T+V_2 & \cdot\ \cdot & D_{2,m} & \cdot\ \cdot \\ \cdot & \cdot & \cdot\ \cdot & \cdot & \cdot\ \cdot \\ D_{m,1} & D_{m,2} & \cdot\ \cdot & T+V_m & \cdot\ \cdot \\ \cdot & \cdot & \cdot\ \cdot & \cdot & \cdot\ \cdot \end{pmatrix} \begin{pmatrix} \chi_1^\nu \\ \chi_2^\nu \\ \cdot \\ \chi_m^\nu \\ \cdot \end{pmatrix}. \tag{9}$$

Where $T = -\frac{1}{m_p}\frac{\partial^2}{\partial R^2}$ is the kinetic operator. V_m is the potential-energy surface corresponding to the mth electronic bound state $\phi_m(R, z)$. $D_{m,n}$ is the transition dipole moment between the mth and the nth electronic bound states of the vibrating D_2^+ times the electric field of the external pulse. When FC averaging is included, the total populations of the mth state are $|x_m|^2 = \sum_\nu C_\nu^2 |x_m^\nu|^2$.

A THz pulse, whose time dependent electric component is expressed as $E_T(t) = -\partial A_T(t)/\partial t$ with $A_T(t) = -E_{T0}/\omega_T \sin(\pi t/T_T)^2 \cos(\omega t)$ being the vector potential, can be utilized to realize a high control ratio in the dissociating D_2^+. Here E_{T0}, T_T and ω_T are the strength, pulse duration and central frequency of the THz field, respectively. Then the interaction of D_2^+ with the external laser fields can be described as

$$W(z, t) = \left(1 + \frac{m_e}{2m_p + m_e}\right) z[E_T(t) + E(t - dt)], \tag{10}$$

where dt is the time delay between the on-set of the exciting and the dissociation control (THz) fields. When the on-set of the THz pulse is ahead, dt is positive, otherwise, dt is negative.

3. Simulation results with laser field at 792 nm

3.1. Simulation with TDSE

In this section, a short few-cycle laser pulse with a central wavelength of 792 nm and a duration of 7.7 fs is used to excite the electron wave packets of the initial $1s\sigma_g$ state of the vibrating D_2^+ onto the excited states. The total dissociation probability P_p and the ionization probability P_i of the dissociating D_2^+ versus E_{I0}, the peak electric field strength of the IR laser pulse, are depicted in figure 1 (see the solid red and dashed green curves) (the results obtained with the CEs of the four lowest electric states are also depicted, see the solid gray curve in figure 1, which will be discussed in section 3.2). When the vibrational level corresponding to the initial ground state of the laser induced dissociating H_2^+ is employed as $\nu = 0$, the dissociation probability increases monotonously when the peak intensity of the 800 nm pulse is between 2.0×10^{14} W cm^{-2} (the corresponding strength is 0.075 a.u.) and 7.5×10^{14} W cm^{-2} (0.145 a.u.). In addition, with a further increase of the field strength, the dissociation probability drops monotonously (see figure 5(a) in [15]). Whereas, our results reveal an anomalous dependence of the dissociation probability on the laser strength. Overall, the dissociation degree shows a growing trend with increasing field

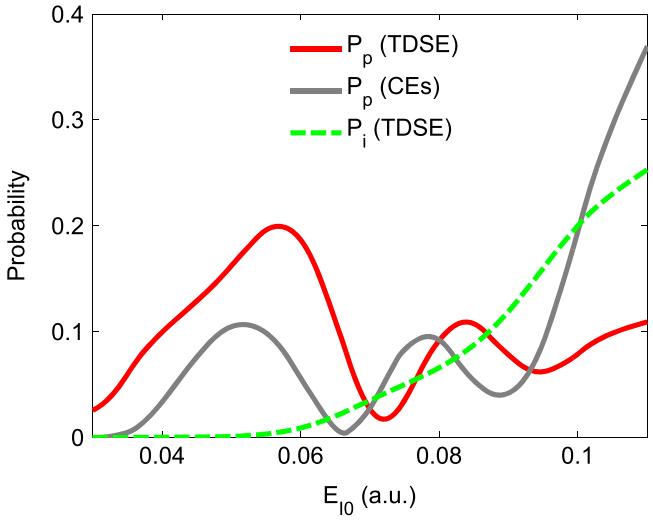

Figure 1. Laser induced dissociation probability P_p and ionization probability P_i of the vibrating D_2^+ as functions of the electric-field strength E_{I0} of the 792 nm laser pulse, whose duration is 7.7 fs. Franck–Condon averaging is included. The populations are obtained with the non-Born–Oppenheimer time-dependent Schrödinger equation (see the solid red and dashed green curves), and the coupled equations of the four lowest electronic states of D_2^+ (see the solid gray curve), respectively.

strength at the beginning, but it oscillates with a further increase of the strength (see the solid red curve in figure 1). Specifically, the dissociation ratio shows a monotonous increase during the initial region, 0.03 a.u. (the corresponding peak intensity is 3.2×10^{13} W cm^{-2}) $\leqslant E_{I0} \leqslant 0.0562$ a.u. (1.12×10^{14} W cm^{-2}). When the strength of the external pulse is $E_{I0} = 0.0562$ a.u. (1.12×10^{14} W cm^{-2}), the dissociation probability reaches its first maximum, 0.206. For intermediate strength values, 0.0562 a.u. (1.12×10^{14} W cm^{-2}) $\leqslant E_{I0} \leqslant 0.0726$ a.u. (1.88×10^{14} W cm^{-2}), the dissociation degree drops monotonously, and there follows the first minimum, reaching 0.0151 at $E_{I0} = 0.0726$ a.u. (1.88×10^{14} W cm^{-2}). As the field strength continues to increase, more oscillations with smaller amplitudes exist when 0.0726 a.u. (1.88×10^{14} W cm^{-2}) $\leqslant E_{I0} \leqslant 0.11$ a.u. (4.31×10^{14} W cm^{-2}). The total ionization probability shows a monotonous increase as the strength of the external pulse increases (see the dashed green curve in figure 1), which is consist with the results in [15]. The increasing ionization probability could drop the total dissociation ratio.

The temporal populations of the four lowest electronic states of D_2^+ as functions of evolution time t are depicted in figure 2. The strength of the IR pulse is 0.0562 a.u. (1.12×10^{14} W cm^{-2}) for figure 2(a) and 0.0726 a.u. (1.88×10^{14} W cm^{-2}) for figure 2(b), respectively. From figure 2 one can find that most populations of all the dissociation events are stabilized at the lowest dissociation state, the $2p\sigma_u$ state, in the photon induced dissociation of the vibrating D_2^+ by the 792 nm IR pulse (see the solid blue curve in figure 2). Few populations are stabilized at the other excited states at the end of the simulation.

In order reveal the underlying mechanism in realizing the strength dependence in the laser-induced dissociation of the vibrating D_2^+, the electron localization probabilities of the twelve lowest vibrational states as functions of the electric-field strength of the IR pulse are demonstrated in figure 3. From this figure one can see clearly that the vibrational levels $\nu = 6-9$ dominantly contribute to the oscillating of the total dissociation probability P_p in figure 1 (see the thick dashed red, thick dashed–dotted green, thick dotted black and thick solid gray curves in figure 3).

Several theoretical models for describing molecules in strong laser fields have been developed. One of the most descriptive models is the Floquet representation [40, 41], which can provide an intuitive insight into the dissociating H_2^+ and its isotopes [6, 13, 44, 51]. The dressed potential energy curves of D_2^+ in the photon field are shown in figure 4. The central wavelength the external pulse is 792 nm. The two lowest electronic states: the attractive $1s\sigma_g$ state and the repulsive $2p\sigma_u$ state are considered, because most electron populations of all the dissociation events are localized at the lowest excited state after the excitation of the IR pulse, see figure 2. The molecular curves must be repeated at all discrete energies of the photon field since D_2^+ and photons are considered as a whole. For low laser intensities (especially without an external field), the molecule ion can be described by diabatic potential curves, which correspond to the potential curves of the two lowest electronic states shifted by n photons (n is the number of photons absorbed) (see the solid gray curves in figure 4). With increasing intensity, the curve crossings become avoided crossings, due to the coupling of the gerade $1s\sigma_g$ and the ungerade $2p\sigma_u$ states by the laser field. A widening energy gap between the upper and lower branches of the so-called, adiabatic potential curves are formed. The adiabatic potential curves for the pulses with peak intensities of 10^{12} W cm^{-2} (the corresponding strength is 0.0053 a.u., see the dashed blue curves in figure 4), 10^{13} W cm^{-2} (0.0168 a.u., the dotted red curves) and 10^{14} W cm^{-2} (0.053 a.u., the solid black curves) are calculated by using 20 Floquet blocks in the present work [44, 51].

As the intensity of the external field increases, the diabatic curves evolve into the adiabatic ones and the 1ω avoided crossing (the crossing at R_1) opens (see the dashed blue curves in figure 4). Any vibrational states whose eigenvalues lie among the energy gap to the dissociative states are allowed. The potential changes from a binding one for $R < R_1$ to a repulsive one for $R > R_1$ when passes through the 1ω crossing. With increasing intensity of the 792 nm pulse, the two adiabatic curves move farther and farther away from their unperturbed position, the 1ω crossing (see the dotted red curve in figure 4). More and more vibrational states become unbound. This lowering of binding potential by laser fields is called BS [1–3]. As the eigenvalues of the vibrational states $7 \leqslant \nu \leqslant 9$ are higher than the asymptotic energy of the final $|u, n-1\rangle$ state (see the solid green line in figure 4), all vibrational states with $7 \leqslant \nu \leqslant 9$ can dissociate. The vibrational state $\nu = 6$ is below the final $|u, n-1\rangle$ state, some amount of dissociation can occur due to the quantum-mechanical tunneling [8] (see the thick dashed red curve in

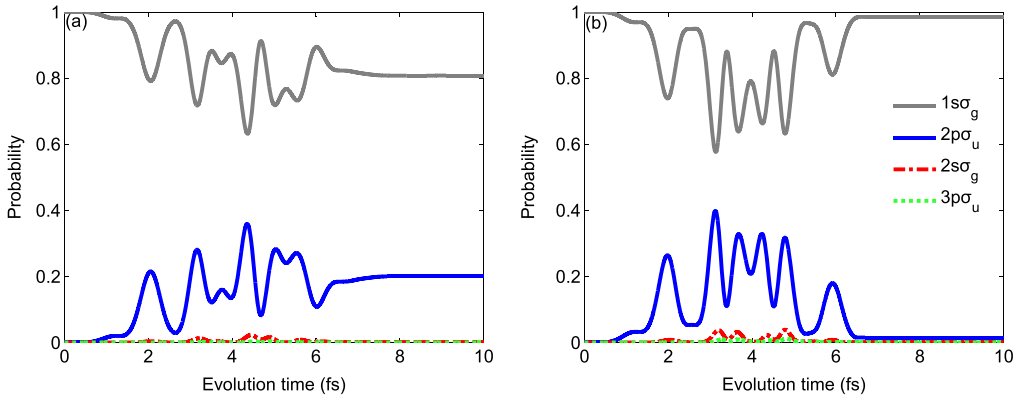

Figure 2. Temporal Franck–Condon-averaged electron populations $D_i(t)$ of the lowest four electronic states of the vibrating D_2^+ as functions of evolution time t. The central wavelength and pulse duration of the external laser pulse are 792 nm and 7.7 fs, respectively. The field strength is 0.0562 a.u. for (a) and 0.0726 a.u. for (b), respectively. The results are obtained with the non-Born–Oppenheimer time-dependent Schrödinger equation.

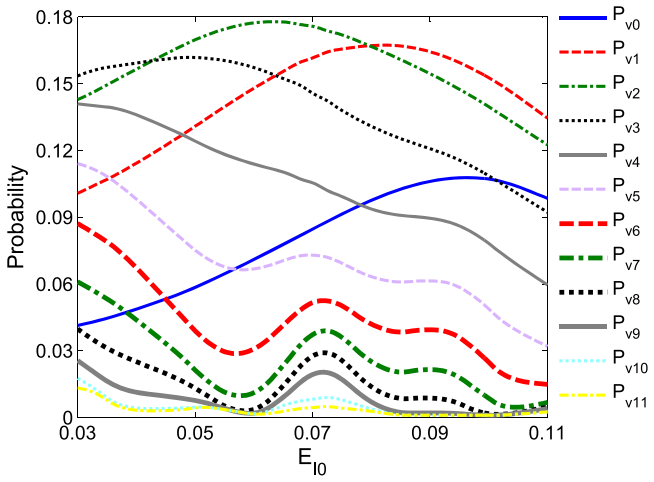

Figure 3. Electron localization probabilities of the twelve lowest vibrational states of the molecular ion D_2^+ after considering Franck–Condon distribution as functions of the electric-field strength of the external pulse, whose central wavelength and duration are 792 nm and 7.7 fs, respectively. The populations are calculated with the non-Born–Oppenheimer time-dependent Schrödinger equation.

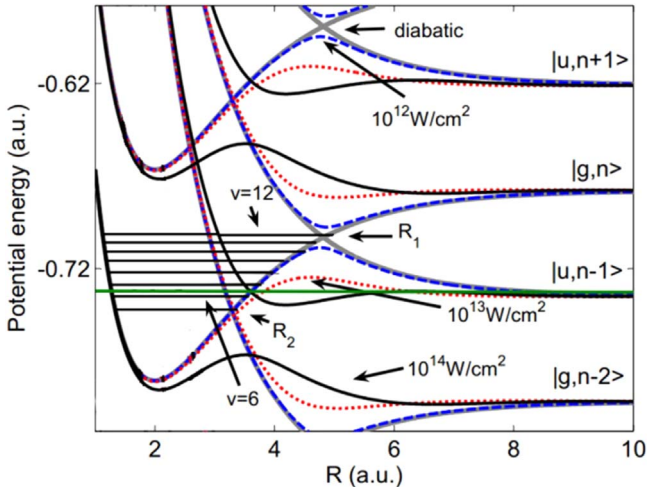

Figure 4. Field-free diabatic (solid gray) and field-dressed adiabatic molecular potential energy curves of D_2^+ for three different intensities. The central wavelength of the external pulse is 792 nm. The adiabatic potential curves for 10^{12} W cm^{-2} (dashed blue), 10^{13} W cm^{-2} (dotted red) and 10^{14} W cm^{-2} (solid black) are calculated by using 20 Floquet blocks.

figure 3). The BS and quantum-mechanical tunneling lead to the population decreasing of the vibrational states of $\nu = 6-9$, and the increase of the dissociation degree, when the strength of the 792 nm pulse is between 0.03 a.u. (3.2×10^{13} W cm^{-2}) and 0.057 a.u. (1.16×10^{14} W cm^{-2}) (see the thick dashed red, thick dashed–dotted green, thick dotted black and thick solid gray curves in figure 3, and the solid red curve in figure 1).

With a further increase of the intensity of the IR pulse, the 3ω avoided crossing (the crossing at R_2) opens (see the solid black curves in figure 4). The actual middle position of the 3ω gap is somewhat lower with respect to the three-photon diabatic crossing. In addition, the one-photon gap at these intensities is so large that it is no longer recognized. Accompanying the creation of a lowering potential crossing, an adiabatic potential well above the energy gap occurs at each avoided crossing. The wave packets of the vibrational states with higher eigenvalues ($\nu \geqslant 6$) slow down in the shallow part of the adiabatic potential well above the 3ω avoided crossing, and can be trapped in such a laser-induced adiabatic well, because most of the wave packets cross the gap diabatically [52]. This phenomenon is referred to as BH [4–6]. Strictly speaking, the Floquet formalism describes the interaction of a molecule with an infinitely monochromatic wave. It is well suited when the pulse envelope changes slowly compared to the nuclear dynamics. For ultrashort laser pulses, the envelope has to be taken into account when considering the dynamics of the wave packet on the adiabatic curves [51]. As the intensity decreases in the falling edge of our short few-cycle laser pulse, the shape of the adiabatic potential well above the 3ω avoided crossing changes from concave to convex. It becomes the bottom part of the 1ω avoided crossing. The trapped wave packets can move back to the $1s\sigma_g$ state or dissociate with almost zero energy [6]. At still higher intensities, multiple oscillations in this adiabatic well above the 3ω gap can occur; this explains the next extrema in P_p versus E_{I0} in figure 1 when

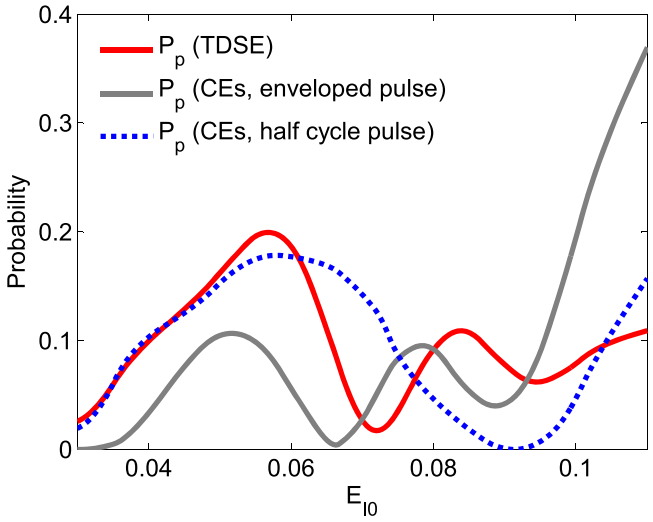

Figure 5. Calculated results with the non-Born–Oppenheimer time-dependent Schrödinger equation and the coupled equations of the four lowest electronic states of D_2^+. The solid red and gray curves are the same as those in figure1. For the dotted blue curve, the central wavelength and duration of the external field are 792 nm and 1.33 fs (half of an optical cycle), respectively.

the strength is between 0.059 a.u. (1.24×10^{14} W cm^{-2}) and 0.11 a.u. (4.31×10^{14} W cm^{-2}) [14].

Compared with the first oscillation lying between 0.03 a.u. (3.2×10^{13} W cm^{-2}) $\leqslant E_{I0} \leqslant$ 0.0726 a.u. (1.16×10^{14} W cm^{-2}), which is induced by the BS and quantum-mechanical tunneling of the 1ω crossing, and the population trapping in the 3ω adiabatic well, the amplitude of the second population oscillation in the dissociating D_2^+ between 0.0726 a.u. (1.88×10^{14} W cm^{-2}) $\leqslant E_{I0} \leqslant$ 0.0948 a.u. (3.2×10^{14} W cm^{-2}) will decrease (see the solid red curve in figure 1), because the second oscillation is triggered by the population oscillating in the three-photon field induced adiabatic potential well. Only part the populations in the adiabatic well will move back to the ground state or dissociate [6].

3.2. Simulation with coupled equations

As can be found in figure 2, with the 792 nm IR pulse, most populations of all the dissociation events are localized at the lowest dissociation state, the ungerade $2p\sigma_u$ state, at the end of the simulation. Whereas, some populations are stabilized at the $2s\sigma_g$ and $3p\sigma_u$ states during the dissociation process, especially with a strong IR pulse (see figure 2(b)). To further demonstrate the electron dynamical behavior in the dissociation of the vibrating molecular ion D_2^+, we consider the CEs among the lowest four states. The obtained dissociation population P_p of the dissociating D_2^+ versus E_{I0} is depicted as the solid gray curve in figure 5 (this curve is also depicted in figure 1, see the solid gray curve in figure 1) (as comparison, the dissociation population curve obtained with TDSE is also depicted in figure 5, see the solid red curve, which is the same as the solid red curve in figure 1). The same as the results obtained with TDSE, P_p calculated with CEs of the four lowest states also oscillates with increasing intensity of the IR field (see the solid red and gray curves in figure 5). Whereas, there show some discrepancies between the two models in terms of the field strengths giving maxima/minima of dissociation probability and the relative dissociation yields. For instance, with TDSE, the dissociation probability reaches its first maximum, 0.206 when the strength of the IR pulse is $E_{I0} = 0.0562$ a.u. (1.12×10^{14} W cm^{-2}). And when $E_{I0} = 0.0726$ a.u. (1.88×10^{14} W cm^{-2}), the dissociation degree reaches the first minimum 0.0151. While with the CEs of the four lowest electric states of D_2^+, the dissociation degree reaches its first maximum 0.1063 at $E_{I0} = 0.0524$ a.u. (0.977×10^{14} W cm^{-2}), and there follows the first minimum 0.0044 when $E_{I0} = 0.0667$ a.u. (1.58×10^{14} W cm^{-2}). Additionally, with TDSE, the total ionization probability shows a monotonous increase as the strength of the IR pulse increases, and the increased ionization probability could drop the total dissociation ratio. However, ionization is not considered in the CEs, the dissociation probability shows a monotonous increase when the strength of the IR pulse is larger than 0.0993 a.u. (3.51×10^{14} W cm^{-2}, see the solid gray curve in figure 5).

When illuminated by laser fields, the populations of a two-level atom may stay in the upper or lower levels periodically by absorbing or emitting photons. This is usually called Rabi oscillation [28]. Rabi oscillation can also occur in molecules [29–33], which includes free–free Rabi oscillation, happening between two excited states [31], and bound-free Rabi oscillation, taking place between the ground state and the first electronically excited state [32]. The temporal population in one state of an atom or a molecule is roughly proportional to $\sin^2(\Omega_R t/2 + \alpha)$. Here Ω_R is the Rabi frequency, which is dependent on the strength of the interaction field, and the dipole moment induced between the two atomic or molecular energy levels. α is the carrier phase of the oscillation. In molecules, several Rabi oscillations may coexist, especially with a short enveloped pulse laser. There is a relation between the pulse duration and the width of the spectrum. The shorter pulse duration, the broader is the maximal frequency spectrum that can be obtained [45]. The energy curves of D_2^+ are continuous, and when illuminated by a resonant short pulse laser, transitions among the lower and upper energy levels will in general have several different transition moments and hence different Rabi frequencies, which will lead to some complicated phenomena, e.g. the damping of the Rabi oscillations (especially when the dissociation control field is not strong enough), which have been demonstrated both theoretically and experimentally [53, 54]. In order to shed some light on the field intensity effect on the laser induced dissociation of the vibrating D_2^+, we employ a half optical cycle 792 nm pulse to conduct the simulation with the CEs of the lowest four electronic states. As the results obtained with an enveloped IR pulse (both with TDSE and CEs, see the solid red and gray curves in figure 5), the obtained dissociation probabilities are also oscillating with increasing strength of the IR pulse (see the dotted blue curve in figure 5), though the three curves are not perfectly consistent with each other, as shown in figure 5.

The Rabi oscillations between the two lowest electronic states of D_2^+ can be clearly seen in the temporal states

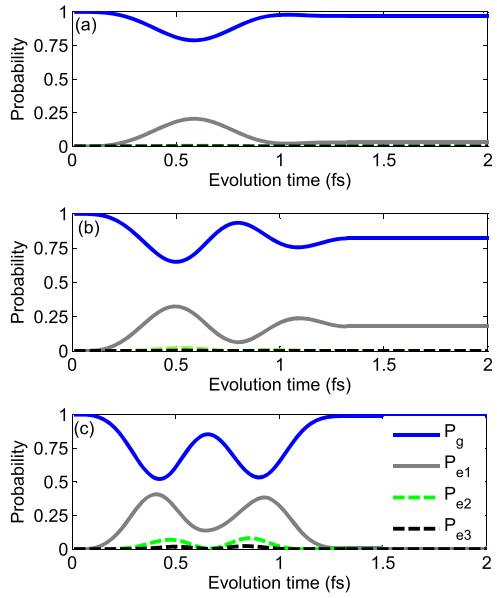

Figure 6. Temporal populations of the lowest four electric states of D_2^+ as functions of evolution time t. The results are calculated with the coupling of the four lowest electronic states, and the central wavelength and pulse duration of the external field are 792 nm and 1.33 fs (half of an optical cycle), respectively. The field strength is 0.03 a.u. for (a), 0.058 a.u. for (b) and 0.092 a.u. for (c), respectively.

populations, as shown in figure 6. The Rabi frequency Ω_R is dependent on $D_{gu}(R)$, the transition dipole moment $d_{gu}(R)$ between the $1s\sigma_g$ and $2p\sigma_u$ states, times E_{I0}, the strength of the IR pulse. With increasing IR pulse strength, Ω_R will increase, which can lead to a reduced population oscillating period (see the solid blue and gray curves in figure 6). For instance, when the strength of the IR pulse is 0.03 a.u. (0.32×10^{14} W cm^{-2}), the population oscillating period lasts about 1.03 fs, and when $E_{I0} = 0.058$ a.u. (1.2×10^{14} W cm^{-2}), the oscillating period reduces to 0.8 fs. The entire pulse duration of the IR pulse (the total duration of the Rabi oscillation) lasts about 1.33 fs. The changes in Rabi frequency will lead to the oscillating of the dissociation populations of the vibrating D_2^+ with increasing intensity of the IR pulse.

4. Simulation results with laser field at 198 nm

In this section, we consider an exciting pulse with a central wavelength of 198 nm. The duration of this short few-cycle UV pulse lasts about 7.7 fs, which is same as that of the 792 nm pulse in the above section.

Most populations of all the dissociation events are localized at the lowest excited state, the $2p\sigma_u$ state, after the exciting of the IR pulse, see figure 2. While, with increasing strength E_{u0} of the 198 nm pulse, populations of the ground state of the vibrating D_2^+ can be transferred onto higher excited states with a multiphoton transition, as can be found in figure 7. The populations are obtained with the non-BO TDSE (see the thick curves in figure 7) and the coupling among the six lowest electronic states of D_2^+ (see the thin curves in figure 7), respectively.

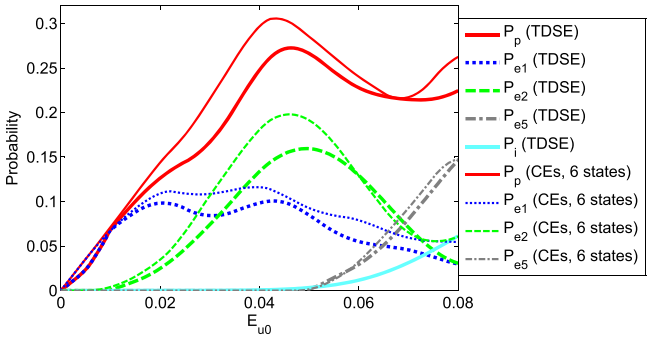

Figure 7. Franck–Condon-averaged dissociation probability P_p and populations of the $2p\sigma_u$ (P_{e1}), $2s\sigma_g$ (P_{e2}) and $4f\sigma_u$ (P_{e5}) states of the molecular ion D_2^+ as functions of the electric-field strength of the 198 nm laser pulse, whose duration is 7.7 fs. The populations are obtained with the non-Born–Oppenheimer time-dependent Schrödinger equation, see the thick curves, and the coupled equations of the six lowest electronic states of D_2^+, see the thin curves, respectively. The thick solid cyan curve is the ionization probability P_i obtained with the time-dependent Schrödinger equation.

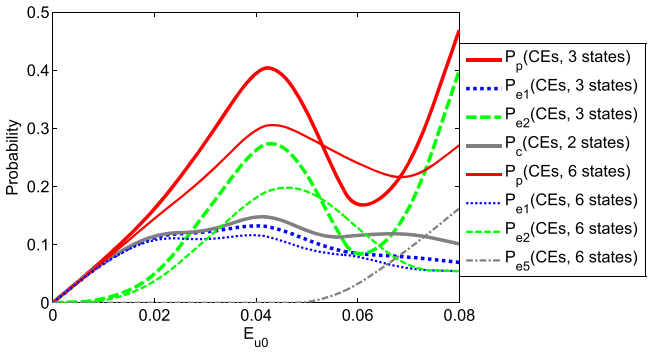

Figure 8. Same as the thin curves in figure 7 (these four thin curves are also depicted here in order to compare the differences when changing the number of coupled states) except the coupled equations are changed into the coupling among the three lowest electronic states. For comparison, the solid gray curve depicts the strength dependence of the total dissociation probability P_c when the two lowest electronic states are considered.

At low strengths, the absorption dynamics rather proceeds via a one-photon jump from the initial $1s\sigma_g$ state onto the $2p\sigma_u$ state (see the dotted blue curves in figure 7). The dissociation degree shows a mnotonous increase with increasing strength of the UV pulse. For intermediate strength values, the dominant feature corresponds to the two-photon absorption. Most populations of all the dissociation events absorb two photons, and are excited onto the $2s\sigma_g$ state (see the dashed green curves in figure 7). The total dissociation probability reaches its first peak value, and then drops with decreasing dissociation probability of the two-photon channel. Above $E_{u0} = 0.05$ a.u. (8.9×10^{13} W cm^{-2}), the dissociation probability toward the three-photon channel increases to such an extent that for $E_{u0} = 0.068$ a.u. (1.65×10^{14} W cm^{-2}), it is the same order of the two-photon channel, and for higher strength values, it describes the dominant process (see the dashed–dotted gray curves in figure 7). In short, with increasing strength of the 198 nm pulse, the dissociation populations of D_2^+ oscillate, a

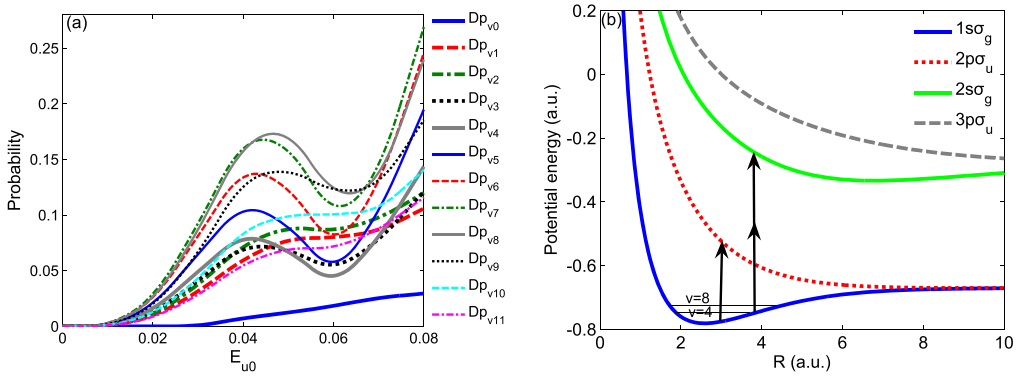

Figure 9. (a) Populations Dp_{vi} of the $2s\sigma_g$ state as functions of the UV field strength. The initial vibrational state is the ith level, and i equals to 0, 1, 2, 3, 4, …, 11. The central wavelength and pulse duration of the UV pulse are 198 nm and 7.7 fs, respectively. (b) The four lowest potential energy curves of the molecular ion D_2^+.

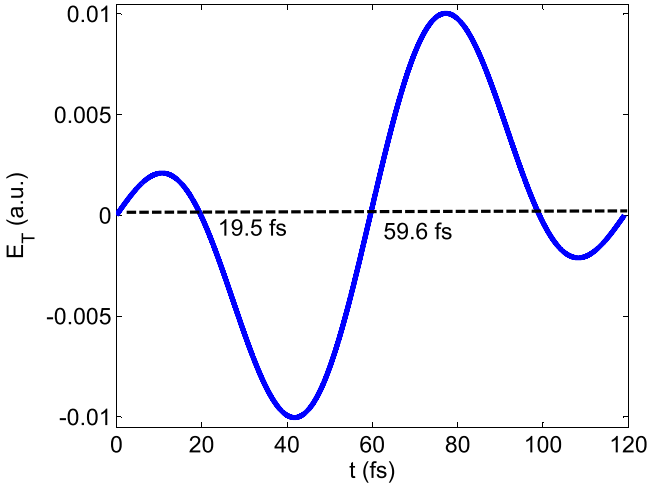

Figure 10. Electronic field of the dissociation control THz field, whose central wavelength, strength and duration are 36 μm, 0.01 a.u. and 120 fs, respectively.

similar conclusion as that obtained with the 792 nm pulse, even though the amplitude of the oscillation decreases. For simplicity, we just consider the four lowest electronic states in the present work. The three-photon channel is induced by electron transition between the initial $1s\sigma_g$ state and the $4f\sigma_u$ state, the sixth lowest state, which is not considered in the present study.

With the CEs of the three lowest electronic states of the vibrating D_2^+, one can see clearly that the two-photon transition dominates the dissociation probability oscillations (see the thick solid red and thick dashed green curves in figure 8). Compared with the results obtained with the CEs of the six lowest electronic states, one can find that P_p oscillates more violently without the higher $4f\sigma_u$ state, because the two-photon transition oscillates more obviously without the three-photon channel (see the thick and thin solid red curves, and the thick and thin dashed green curves in figure 8). The vibration of the one-photon transition between the $1s\sigma_g$ and $2p\sigma_u$ states with varying strength is weak (see the thick dotted blue curve in figure 8). For reference, the dependence of the total dissociation probability P_c obtained with the coupling of the two lowest electronic states, on the UV pulse strength is depicted (see the thick solid gray curve in figure 8). With a weak UV pulse, the two population curves, P_{e1} (obtained with CEs of the lowest three electric states, see the thick dotted blue curve) and P_c, overlap. There just shows some small differences as the field strength increases. The population localization probabilities of the $2p\sigma_u$ state change slightly with and without the $2s\sigma_g$ state. Populations of the $2s\sigma_g$ state are dominantly from the initial $1s\sigma_g$ state through a two-photon transition, rather than from the $2p\sigma_u$ state by another one-photon transfer.

The laser induced electron transition between the $1s\sigma_g$ and $2s\sigma_g$ states is through a two-photon transfer. Therefore, the Floquet representation is no longer applicable. When the initial state is chosen as the ith vibrational level, one can find that the oscillating populations of the $2s\sigma_g$ state with increasing strength of the UV pulse are dominantly from levels $\nu = 4-8$, as can be found in figure 9(a). The energy gaps between these vibrational states and the $2s\sigma_g$ state at the equilibrium internuclear distances are close to the two-photon energy of the 198 nm UV pulse, as can be seen in figure 9(b). The Rabi oscillations can take place. The populations of states $\nu = 4-8$ can be resonantly transferred onto the excited $2s\sigma_g$ state by absorbing two photons of the 198 nm UV pulse. Meanwhile, the electron wave packets of the $2s\sigma_g$ state can also be transferred back to levels $\nu = 4-8$ through emitting two photons of the UV pulse. The Rabi frequency Ω_R is dependent on the strength of the interaction field, which will lead to oscillating populations of the $2s\sigma_g$ state as the strength of the UV pulse increases.

5. Electron localization control with a THz pulse

In this section, a THz pulse, whose central wavelength, strength and duration are 36 μm, 0.01 a.u. (3.56×10^{12} W cm^{-2}) and 120 fs, respectively (detail information in figure 10), is utilized to steer the electron motion of the dissociating D_2^+ after the excitation of the 792 nm IR pulse and the 198 nm UV pulse, respectively.

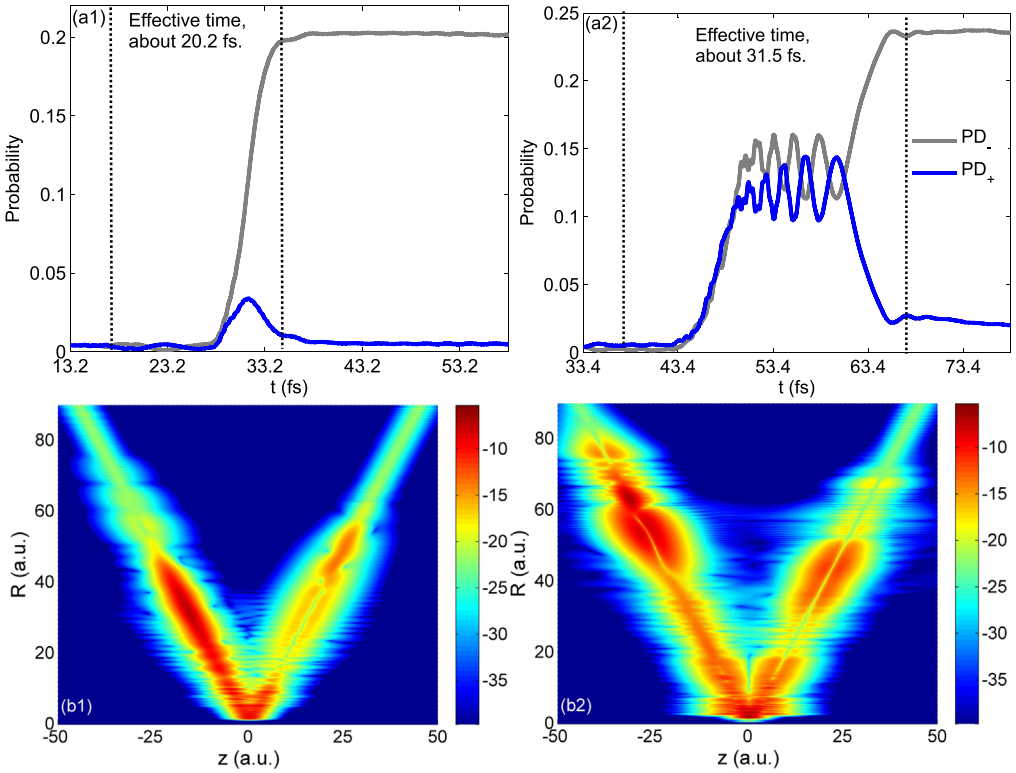

Figure 11. Upper panel: temporal electron probabilities of the right (PD_+) and left (PD_-) nuclei as functions of evolution time t after considering Franck–Condon distributions. Lower panel: snapshots of the common logarithm of the electron- nuclear probability density distribution obtained with a 36 μm THz pulse after the exciting of a 792 nm pulse ((b1), the pulse duration is 7.7 fs, and the strength is 0.058 a.u.), or a 198 nm pulse ((b2), the pulse duration is 7.7 fs, and the strength is 0.046 a.u.), taken at the end of the simulation. The strength and duration of the dissociation control THz pulse are 0.01 a.u. and 120 fs, respectively. The time delay of these two pulses is 13.2 fs for (a) and 33.4 fs for (b), respectively.

Figure 11 shows the temporal electron localization probabilities $PD_\pm$ of the right (PD_+) and left (PD_-) potential wells as functions of evolution time t [42], and the snapshots of the common logarithm of the electron-nuclear probability density distribution taken at the end of the simulation. For the left panels, the central wavelength, pulse duration and strength of the exciting field are 792 nm, 7.7 fs and 0.058 a.u. (1.2×10^{14} W cm^{-2}), respectively. The time delay of the IR and THz pulses is $dt = 13.2$ fs. For the right panels, a UV pulse with a central wavelength of 198 nm, a duration of 7.7 fs and a strength of 0.046 a.u. (7.53×10^{13} W cm^{-2}) is employed to excite the molecular ion before the dissociation control of the THz field. The time delay of the UV and THz pulses is chosen as $dt = 33.4$ fs.

With the two-pulse scheme of the IR and THz spectral regimes, most populations of all the dissociation events are steered to the left potential well during the effective time window for the laser induced dissociation control of the vibrating molecular ion D_2^+, which lasts about 20.2 fs, as can be seen in figure 11(a1). One can find that the populations of the left and right potential wells are $PD_- = 0.202$, respectively, $PD_+ = 0.005$ when the system is stable. 97.6% populations of all the dissociation states are localized at the left nucleus, as can be found in figure 11(b1).

When the exciting pulse is changed into the short 198 nm UV pulse, most populations of all the dissociation events can also be steered onto the left potential well in figure 11(b2), which is the same as that obtained after the exciting of the IR pulse. Whereas, more populations can be excited onto higher dissociation states under the exciting of the UV pulse, which will lead to a more complicated simulation result. As shown in figure 11(a2), populations of the two potential wells are comparable at the beginning of the effective dissociation control time window, which is changed into 31.5 fs. Then the dissociation populations oscillate between the two wells during the middle period of the time window. Finally, most populations are steered onto the left nucleus and stabilized at the last period of the time window. One can obtain that $PD_- = 0.234$ and $PD_+ = 0.02$ when stable. 92.1% populations of all the dissociation events are localized at the left potential well at the end of the simulation, see figure 11(b2).

To explore the underlying mechanism in realizing the laser induced dissociation control of the vibrating D_2^+, the temporal populations $D_i(t)$ of the four lowest electronic states are demonstrated. With the 792 nm pulse, most populations of all the dissociation states are stabilized at the $2p\sigma_u$ state, as shown in figure 12(a). When the time delay of the 792 nm IR and the 36 μm THz pulses is $dt = 13.2$ fs, the effective time window for the dissociation control starts at $t = 17.1$ fs, and ends at $t = 37.3$ fs, which lasts about 20.2 fs (as can be found in figure 11(a1)). When the evolution time lies between 19.5 and 37.3 fs, the electric field of the THz field is $E_T < 0$ (see

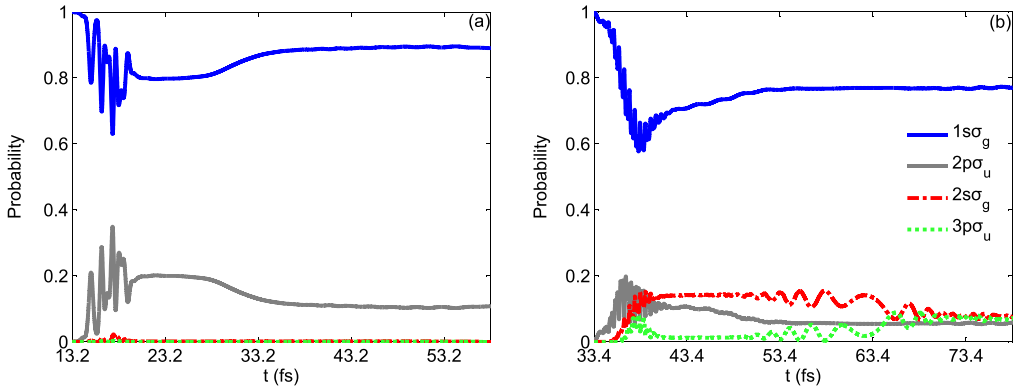

Figure 12. Same as the upper panels in figure 11, except the temporal electron probabilities of $PD_{\pm}$ are changed into the temporal populations $D_i(t)$ of the four lowest electronic states of the molecular ion D_2^+.

figure 10), the left potential well of the dissociating D_2^+ is ascended and the right one is descended. For the populations of the dissociative state $2p\sigma_u$, they move oppositely to the electric field force direction and are stabilized at the dressed-up potential well, the left one, at the end of the simulation [55].

When the time delay of the 198 nm UV and the THz fields is $dt = 33.4$ fs, about 39.7% and 55.5% populations of all the dissociation events are localized at the $2p\sigma_u$ and the higher $2s\sigma_g$ states at the end of the simulation, respectively, as shown in figure 12(b). The effective time for the dissociation control starts at $t = 37.3$ fs, and ends at $t = 68.8$ fs, which lasts about 31.5 fs. When 37.3 fs $\leqslant t \leqslant$ 59.6 fs, the electric field of the THz pulse is $E_T < 0$, the left potential well is dressed-up and the right one is dressed-down. Populations of the $2p\sigma_u$ state move oppositely to the THz field and are stabilized at the dressed-up potential well, the left one, before $t \leqslant 57.5$ fs, because the effective dissociation control time window for the populations of the $2p\sigma_u$ state lasts about 20.2 fs. Whereas, for the populations of the $2s\sigma_g$ state, they move along the THz field, and need a longer time to be stabilized [50]. When 59.6 fs $\leqslant t \leqslant$ 68.8 fs, the THz field is $E_T > 0$, the right potential well is ascended and the left one is descended. Populations of the $2s\sigma_g$ state move along the THz field and are localized at the left nucleus at the end of the simulation. At last, 92.1% populations of all the dissociation states can be stabilized at the left potential well when stable.

6. Summary and conclusion

In conclusion, we have shown the field intensity effect on the laser induced dissociation of the vibrating D_2^+ in intense laser pulses at two central wavelengths: 792 and 198 nm by numerically solving the non-BO TDSE and the CEs among electronic states. The dissociation degree oscillates with increasing intensity of the external field. For the IR pulse, most populations of all the dissociation events are stabilized at the lowest excited state, both the Floquet representation and the Rabi oscillations can be employed to disclose the underlying mechanism of the population oscillating. Whereas, for the 198 nm UV pulse, the $2s\sigma_g$ state dominantly contributes to the population oscillating. The electron transition between the $1s\sigma_g$ and $2s\sigma_g$ states is a two-photon transfer, the Floquet representation is no longer applicable. The energy gaps between the vibrational levels $\nu = 4-8$ and the $2s\sigma_g$ state at the equilibrium internuclear distances are close to the two-photon energy of the UV pulse, and the Rabi oscillations can be produced. Populations of the $2s\sigma_g$ state will be increased or decreased through absorbing or emitting two photons of the UV pulse. A THz pulse can realize a high control ratio in the laser induced dissociating of the vibrating D_2^+ molecular ion after the exciting of the IR and UV pulses. For instance, when a single cycle 36 μm THz pulse is used to steer the electron motion after the exciting of the two pulses, about 97.6% and 92.1% populations of all the dissociation states can be stabilized at one potential well at the end of the simulation, respectively.

Acknowledgments

The authors acknowledge valuable discussions with Professor Yanjun Chen of Shaanxi Normal University and Yunpei Deng of Paul Scherrer Inst. This work was supported by the National Natural Science Foundation of China (Grant Nos. 11604349, 61675118) and the Scientific Research Foundation of Shandong University of Science and Technology for Recruited Talents (Grant No. 0104060511610).

ORCID iDs

Z M Jia https://orcid.org/0000-0002-2677-3146
Y D Peng https://orcid.org/0000-0002-5376-0308

References

[1] Zavriyev A, B ucksbaum P H, Muller H G and Sc humacher D W 2000 *Phys. Rev.* A **42** 5500
[2] Bucksbaum P H, Zavriyev A, Muller H G and Schumacher D W 1990 *Phys. Rev. Lett.* **64** 1883
[3] Gopal R *et al* 2009 *Phys. Rev. Lett.* **103** 053001
[4] Allendorf S W and Szöke A 1991 *Phys. Rev.* A **44** 518
[5] Zavriyev A and Bucksbaum P H 1993 *Phys. Rev. Lett.* **70** 1077

[6] Frasinski L J, Posthumus J H, Plumridge J, Codling K, Taday P F and Langley A J 1999 *Phys. Rev. Lett.* **83** 3625
[7] Ergler T, Rudenko A, Feuerstein B, Zrost K, Schröter C D, Moshammer R and Ullrich J 2006 *Phys . Rev. Lett.* **97** 193001
[8] Giusti-Suzor A, He X, Atabek O and Mies F H 1990 *Ph ys. Rev. Lett.* **64** 515
[9] Esry B D, Sayler A M, Wang P Q, Carnes K D and Ben-Itzhak I 2006 *Phys. Rev. Lett.* **97** 013003
[10] Giusti-Suzor A and Mies F H 1992 *Phys. Rev. Lett.* **68** 3869
[11] Posthumus J H, Plumridge J, Frasinski L J, Codling K, Divall E J, Langley A J and Taday P F 2000 *J. Phys. B: At. Mol. Opt. Phys.* **33** L536
[12] Feuerstein B and Thum m U 2003 *Phys. Rev.* A **67** 063408
[13] Giusti-Suzor A, Mies F H, DiMauro L F, Cha rron E and Yang B 1995 *J. Phys. B: At. Mol. Opt. Phys.* **28** 309–39
[14] Aubanel E E, Conjus teau A and Bandrauk A D 1993 *Phys. Rev.* A **48** R4011
[15] Liu K, Hong W, Zhang Q and Lu P 2011 *Opt. Express* **19** 26359
[16] Urbain X, Fabre B, Staicu-Casagrande E M, Ruette N, de, Andrianarijaona V M, Jureta J and Posthumus J H 2004 *Phys. Rev. Lett.* **92** 163004
[17] Nabekawa Y, Furukawa Y, Okino T, Eilanlou A A, Takahashi E J, Yamanouchi K and Midorikawa K 2015 *Nat. Commun.* **6** 8197
[18] Murphy D S, McKenna J, Calvert C R, Williams I D and McCann J F 2007 *New J. Phys.* **9** 260
[19] Williams I *et al* 2000 *J. Phys. B: At. Mol. Opt. Phys.* **33** 2743
[20] Wang P Q, Sayler A M, Carnes K D, Xia J, Smith M A, Esry B D and Ben-Itzhak I 2005 *J. Phys. B: At. Mol. Opt. Phys.* **38** L251
[21] Ben-Itzhak I, Wang P Q, Xia J, Sayler A M, Smith M A, Carnes K D and Esry B D 2005 *Phys. Rev. Lett.* **95** 073002
[22] Kling *et al* 2006 *Science* **312** 246
[23] Tong X M and Lin C D 2007 *Phys. Rev. Lett.* **98** 123002
[24] Roudnev V and Esry B D 2007 *Phys. Rev.* A **76** 023403
[25] Abeln B, Hernández J V, Anis F and Esry B D 2010 *J. Phys. B: At. Mol. Opt. Phys.* **43** 155005
[26] Hua J J and Esry B D 2009 *J. Phys. B: At. Mol. Opt. Phys.* **42** 085601
[27] Manuel K *et al* 2009 *Phys. Rev. Lett.* **103** 213003
[28] Scully Marlan O and Zubairy Suhail M 1997 *Quantum Optics* (Cambridge: Cambridge University Press) pp 152–5
[29] Qi J, Spano F C, Kirova T, Lazoudis A, Magnes J, Li L, Narducci M, Field R W and Lyyra A M 2007 *Phys. Rev. Lett.* **88** 173003
[30] Palacios A, Bachau H and Martín F 2007 *Phys. Rev.* A **75** 013408
[31] Magnier S, Persico M and Rahman N 1999 *Phys. Rev. Lett.* **83** 2159
[32] Granucci G, Magnier S and Persico M 2002 *J. Chem. Phys.* **116** 1022–9
[33] You X Y and Feng H 2014 *Phys. Rev.* A **89** 063405
[34] Kling M F, Siedschlag C, Znakovskaya I, Verhoef A J, Zherebtsov S, Krausz F, Lezius M and Vrakking M J J 2008 *Mol. Phys.* **106** 455
[35] Sansone G *et al* 2010 *Nature* **465** 763
[36] Fischer B, Kremer M, Thomas P, Bernold F, Vandana S, Uwe T, Dieter S C, Robert M and Joachim U 2010 *Phys. Rev. Lett.* **105** 223001
[37] Calvert C R, King R B, Bryan W A, Newell W R, McCann J F, Greenwood J B and Williams I D 2010 *J. Phys. B: At. Mol. Opt. Phys.* B **43** 011001
[38] Xue S, Du H C, Yue S J, Wu H M and Hu B T 2017 *Chin. Phys.* B **26** 058201
[39] Lan Pengfei T E J, Kunlong L, Yuxi F and Katsumi M 2013 *New J. Phys.* **15** 063023
[40] Shirley J H 1965 *Phys. Rev.* **138** B979
[41] Chu S I 1981 *J. Chem. Phys.* **75** 2215
[42] Jia Z, Zeng Z, Li R, Xu Z and Deng Y 2014 *Phys. Rev.* A **89** 023419
[43] He F 2012 *Phys. Rev.* A **86** 063415
[44] He F, Ruiz C and Becker A 2007 *Phys. Rev. Lett.* **99** 083002
[45] Fischer B 2010 Time resolved studies of H_2^+ dissociation with phase-stabilized laser pulses *PhD Thesis* University of Heidelberg, Germany Combined Faculties for the Natural Sciences and for Mathematics of the Ruperto-Carola (https://doi.org/10.11588/heidok.00010756)
[46] Roudnev V, Esry B D and Ben-Itzhak I 2004 *Phys. Rev. Lett.* **93** 163601
[47] Kosloff R and Tal-Ezer H 1983 *Chem. Phys. Lett.* **127** 223–30
[48] Dunn Gordon H 1966 *J. Chem. Phys.* **44** 2592
[49] Hermann M R and Fleck J A Jr 1988 *Phys. Rev.* A **38** 6000
[50] Jia Z and Peng Y 2019 *J. Phys. B: At. Mol. Opt. Phys.* **52** 015603
[51] Pavičić Domagoj 2004 Coulomb explosion and intense-field photodissociation of ion-beam H_2^+ and D_2^+ *PhD Thesis* der Ludwig-Maximilians-Universität, München, Germany
[52] Bandrauk A D 1994 *Molecules in Laser Fields* (New York: Dekker) (https://doi.org/10.1007/978-94-011-0345-9_6)
[53] Shore B W 1978 *Phys. Rev.* A **l7** 1739
[54] Delsart C and Keller J-C 1976 *J. Phys. B: At. Mol. Opt. Phys.* **9** 2769
[55] Jia Z, Zeng Z, Li R and Xu Z 2016 *J. Phys. B: At. Mol. Opt. Phys.* **49** 215604